A two-dimensional nitrogen and carbon flux model in a coastal upwelling region

Debby Ianson[1] and Susan E. Allen

Earth and Ocean Sciences Department, University of British Columbia, Vancouver, British Columbia, Canada

Received 9 May 2001; revised 2 November 2001; accepted 2 November 2001; published 23 February 2002.

[1] Coastal upwelling regions are associated with high primary production and disproportionately large fluxes of organic matter relative to the global ocean. However, coastal regions are usually homogenized in global ocean carbon models. We have developed a carbon and nitrogen flux model including all major processes both within and below the euphotic zone over seasonal to decadal timescales for coastal upwelling regions. These fluxes control surface pCO_2. The model is applied to the west coast of Vancouver Island, Canada (~49°N, 126°W). Net annual air-sea CO_2 exchange and export flux of inorganic and organic carbon and nitrogen from the system to the rest of the ocean are estimated for different model scenarios. Model sensitivities are discussed. Results show strong biological drawdown of pCO_2 during summer and atmospheric CO_2 invasion. However, this invasion is nearly balanced by gas evasion during winter. Therefore the region is a much smaller sink of atmospheric CO_2 (6 g C $m^{-2}yr^{-1}$, or equivalently 200 kg C yr^{-1} per m coastline) than the summer season predicts. More significantly, there is a large flux of inorganic carbon (3×10^4 kg C yr^{-1} per m coastline) from intermediate depth ocean water to the surface ocean via the coastal system compared to a small export of organic carbon (all dissolved) (2×10^3 kg C yr^{-1} per m coastline) back into the lower layer of the open ocean. Thus we suggest that the dominant effect of coastal upwelling on the global ocean is providing a conduit for inorganic carbon to the surface ocean. *INDEX TERMS:* 4219 Oceanography: General: Continental shelf processes; 4516 Oceanography: Physical: Eastern boundary currents; 4806 Oceanography: Biological and Chemical: Carbon cycling; 4845 Oceanography: Biological and Chemical: Nutrients and nutrient cycling; *KEYWORDS:* upwelling, downwelling, carbon, coastal, nutrients, export-flux

1. Introduction

[2] It is becoming an accepted fact that the large anthropogenic increase in atmospheric CO_2 is influencing our climate [*Crowley*, 2000], and so great importance is being placed on understanding the global carbon system. The ocean holds the largest active carbon reservoir on Earth [*Siegenthaler and Sarmiento*, 1993] and ultimately sets the atmospheric CO_2 concentration [*Broecker and Peng*, 1982]. Accurate and well-tested oceanic carbon models are required to interpolate sparse data and to predict future CO_2 levels.

[3] Simple ocean box models have demonstrated the importance of biology in setting the carbon capacity of the ocean by drawing down the surface partial pressure of CO_2 (pCO_2) and transporting organic carbon into the deep ocean via sedimenting organic detritus, where remineralization occurs [*Sarmiento*, 1992]. This process has been termed the biological pump [*Volk and Hoffert*, 1985]. A disproportionate amount of carbon is fixed and vertically exported in coastal waters, particularly in upwelling regions [*Eppley and Peterson*, 1979; *Harrison et al.*, 1987]. Therefore it is expected that coastal upwelling regions form an important part of the biological pump.

[4] Despite the global importance of coastal regions, they are seldom included in current global numerical ocean models because resolution is not high enough to deal with the smaller spatial scales and inherent nonhomogeneity. It is one of the major weaknesses of these models [*Doney*, 1999]. Bulk ocean models and budgets have been used to consider coastal processes in a global context. For example, *Christensen* [1994] suggested, using a box model, that over large timescales (thousands of years), coastal denitrification has an important effect on atmospheric pCO_2 and that organic carbon export to the deep sea does not. Another modeling study indicated that net heterotrophy over continental margins has influenced the global carbon budget over the last hundreds of years [*Mackenzie et al.*, 1998]. Also, it has been shown that the effect of terrestrial inputs (particularly anthropogenic) on coastal eutrophication can impact the annual global carbon budget [*Smith and Hollibaugh*, 1993]. *Tsunogai et al.* [1999] suggest that continental shelf areas absorb atmospheric CO_2 and transport it into the subsurface layers of the open ocean based on carbon data from the East China Sea.

[5] Coastal upwelling brings intermediate-depth (100–200 m), nutrient-rich waters to the surface, fueling high primary production [*Smith*, 1994]. These waters also have higher inorganic carbon concentrations and so could be a source of CO_2 to the atmosphere [*Christensen*, 1994]. However, the few inorganic carbon data which have been reported from coastal upwelling regions show strong biological drawdown of pCO_2 and suggest that such regions may be net sinks for atmospheric CO_2 [*Friederich et al.*, 1994; *Simpson*, 1986; *Simpson and Zirino*, 1980]. These studies did not investigate the winter season.

[6] There are detailed physical models of coastal upwelling [e.g., *Allen et al.*, 1995; *Federiuk and Allen*, 1995] and for downwelling [*Allen and Newberger*, 1996]; however, they apply to short timescales. Current computer speed does not allow such

[1]Now at Texas A&M University, College Station, Texas, USA.

0886-6236/02/2001GB001451$12.00

detailed models to be run for full-year simulations. Two-dimensional physical models of an upwelling event have been coupled with nitrogen-based biological models [*Wroblewski*, 1977; *Edwards et al.*, 2000]. Again, biological cycles were not modeled over the winter season and over longer timescales. A primitive equation model [*Haidvogel et al.*, 1991] has been used to simulate circulation in the California Current System. This model has been coupled with an ecological model [*Moisan et al.*, 1996] to investigate offshore transport of phytoplankton by filaments generated in the physical model. There are no previous models specific to coastal upwelling regions which include a carbon cycle.

[7] Furthermore, the current oceanic ecosystem models that we are aware of use fixed C:N (or C:P) ratios to extrapolate carbon fluxes [e.g., *Bacastow and Maier-Reimer*, 1991; *Sarmiento et al.*, 1993], and many carbon models are not predictive but rely on observations (i.e., the relaxation technique [e.g., *Najjar et al.*, 1992]).

[8] We have developed a simple model of a coastal upwelling region which incorporates a biological and a carbon cycle over all seasons for the entire water column. Carbon and nitrogen are not always coupled by a fixed ratio. The system that we are modeling is complex and nonhomogeneous. Furthermore, few measurements exist of many relevant quantities. Thus our primary objective was to develop a model which produced sensible results and then to identify the parameters that strongly influence the system and need to be measured. We provide estimates of net annual primary production (PP), CO_2 gas exchange, and carbon and nitrogen mass exchange between the model system and the open ocean.

2. Model

[9] Our goal is to model the system as simply as possible and obtain reasonable seasonal cycles compared with available data. We only include those processes occurring on timescales of days (weeks) to years that are necessary to determine net carbon fluxes. Horizontally, the model distinguishes between the shelf, slope, and offshore regions, and there are two levels in the vertical (Figure 1a). (The inner shelf is considered only in the upper layer.) The upper layer is the mixed layer where primary production occurs, while in the lower layer, only remineralization occurs. The system has 42 ordinary differential equations, which are solved by a standard Runge-Kutta method [*Press et al.*, 1992] using an adaptive stepper with a time step of 0.1 days or less.

[10] We first define the modeled quantities (state variables) and currencies. Model structure is separated into physical and biological components, and the chemical portion (gas flux calculation) is described last.

2.1. Currencies

[11] Carbon and nitrogen are the two currencies that are used in the model. Carbon is the currency of particular interest, and nitrogen is modeled as the biologically limiting nutrient [*Hutchings et al.*, 1994]. While it is possible that other macronutrients might be limiting at times (e.g., silicic acid [*Dugdale et al.*, 1995]), they occur in such similar ratios (with nitrogen) to the biological demands that choosing one will not greatly affect our model. Micronutrients such as iron are rarely limiting close to the coast (although iron limitation has been observed in coastal California [*Hutchins and Bruland*, 1998]). Each currency has its own set of parameters. Carbon is exchanged at the air-sea interface, whereas nitrogen is not. The dissolved inorganic nitrogen (DIN) pool does not include N_2 or processes involving N_2, such as nitrogen fixation and denitrification.

2.2. State Variables

[12] Three state variables are modeled for each currency (Table 1): dissolved organic (DO), particulate organic (PO) and dissolved inorganic (DI). What is important in the model is whether organic matter sinks or not. Thus the model definition of the DO pool is organic matter which is nonliving and nonsinking, while the nonliving PO pool sinks and so is found only in the lower layer. The living PO pool can control its buoyancy and does not sink, so it stays in the upper layer. Because of the timescales of interest, only the semilabile portion of the total DO (which includes about 30% of the operationally defined DO [*Carlson and Ducklow*, 1995; *Carlson et al.*, 1994]) is modeled. This pool has remineralization timescales of months to years. Labile pools are difficult to estimate and measure and can have faster remineralization rates than the model timescales [*Carlson and Ducklow*, 1995; *Carlson et al.*, 1994]. Fluxes associated with the refractory pool are negligible despite its large size (~70% of the measurable DO matter) because of its long lifetime (order of 1000 years). The difference between PO and DO matter is traditionally defined by standard filter size (0.45 μM), which will make our DO pool larger than the reported semilabile fraction, while our total organic (TO) pools should be comparable after the refractory portion is subtracted. The DI pools include all forms of inorganic materials which are biologically accessible. The DIN pool is made up of nitrate, ammonium and nitrite, and the dissolved inorganic carbon (DIC) pool of bicarbonate, carbonate, and carbon dioxide.

[13] Salinity is modeled as a state variable to tune the physical model and also to determine several quantities (including alkalinity) in the carbonate system necessary to calculate pCO_2. (Nitrate data were also used to tune the physical model [*Ianson*, 2001].)

2.3. Physical Circulation

[14] All state variables are subject to the circulation (Figure 1a) with the exception of PO matter, which is advected (both vertically and horizontally) and mixed horizontally but is not vertically mixed or entrained because of partitioning between viable (nonsinking, upper layer) and nonviable (sinking, lower layer) fractions. Physical parameters and geometry are presented in Table 2.

2.3.1. Advection. [15] Coastal upwelling (flux Up, vertical velocity A, Figure 1a) occurs inside the shelf break [*Lentz*, 1992]. In the model, intermediate-depth water advects from the outer

Figure 1. (opposite) (a) Vertical cross section through a coastal upwelling system showing the geometry of the model. Illustrated are the physical processes: physical advection between shelf, slope, and open ocean with Up representing upwelling flux (Up = Aw_{sh}) and Down representing downwelling flux (Down = Dw_{sh}), where w_{sh} is the width of the shelf box. Input from the inner shelf is shown by B. The vertical mixing fluxes are $M_{Vsh} = M_V w_{sh}$ and $M_{Vsl} = M_V w_{sl}$, where w_{sl} is the width of the slope box. The changes in mixed layer depth between horizontal regions approximate sloping isopycnals. The horizontal mixing fluxes are $M_{H,\,sh\,-\,sl} = M_H h_{sh,\,u}$ and $M_{H,\,sl-oc} = M_H h_{sl,\,u}$ in the upper layer and $M_{H,\,sh-sl} = M_H(h_t - h - u)_{sh}$ and $M_{H,\,sl-oc} = M_H(h_t - h - u)_{sl}$ in the lower layer, where M_H is the horizontal mixing coefficient. (b) The vertical structure of model concentrations using salinity Sas an example. The linear gradient between the upper layer and the permanent pycnocline allows for more realistic vertical entrainment and mixing between layers. (c) The biological model with fluxes shown for the two-layer system using carbon as a currency.

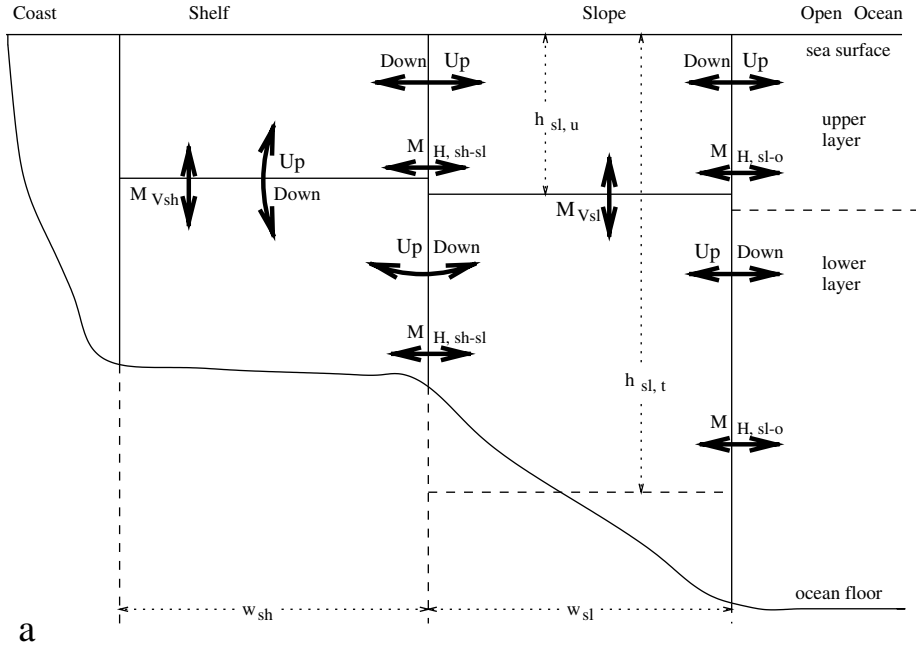
Coast
Shelf
Slope
Open Ocean
sea surface
Down
Up
h sl, u
upper layer
M H, sh-sl
M H, sl-o
Up
Down
M Vsh
M Vsl
Up
Down
Up
Down
lower layer
M H, sh-sl
h sl, t
M H, sl-o
ocean floor
w sh
w sl

a

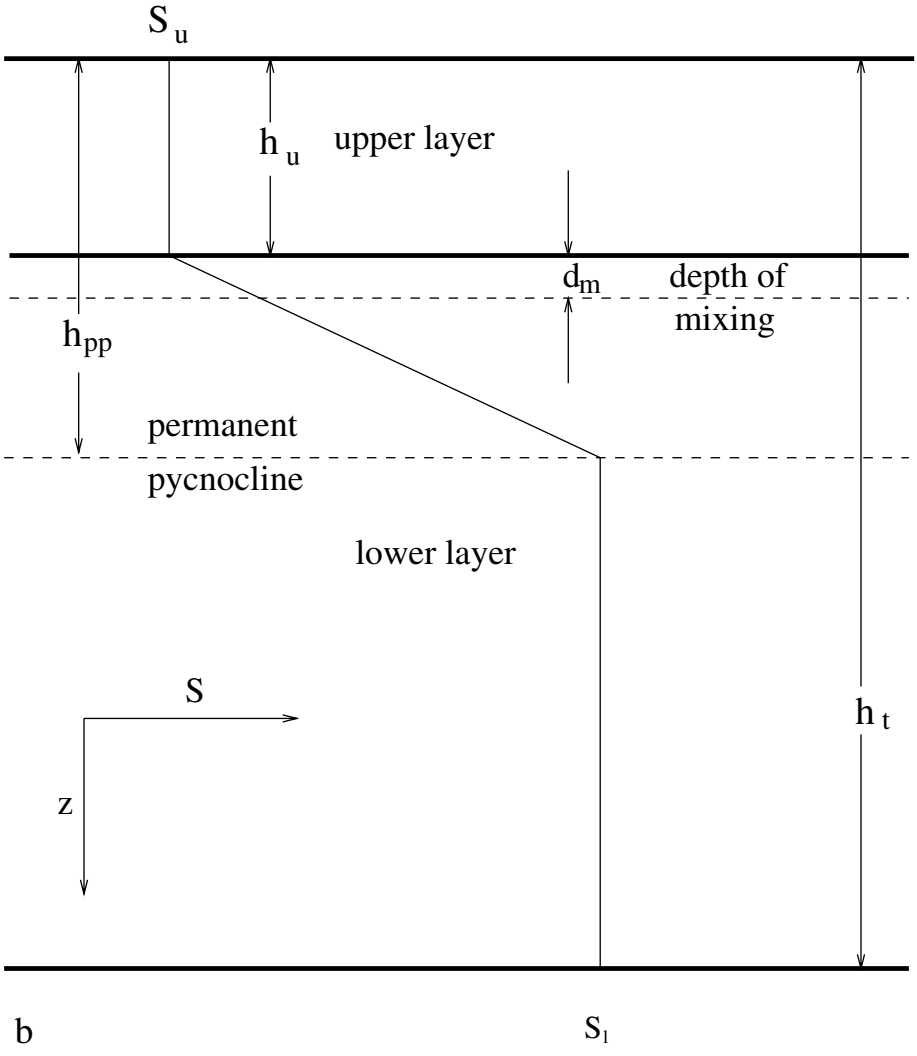
S u
h u
upper layer
d m
depth of mixing
h pp
permanent pycnocline
lower layer
S
z
h t
S l

b

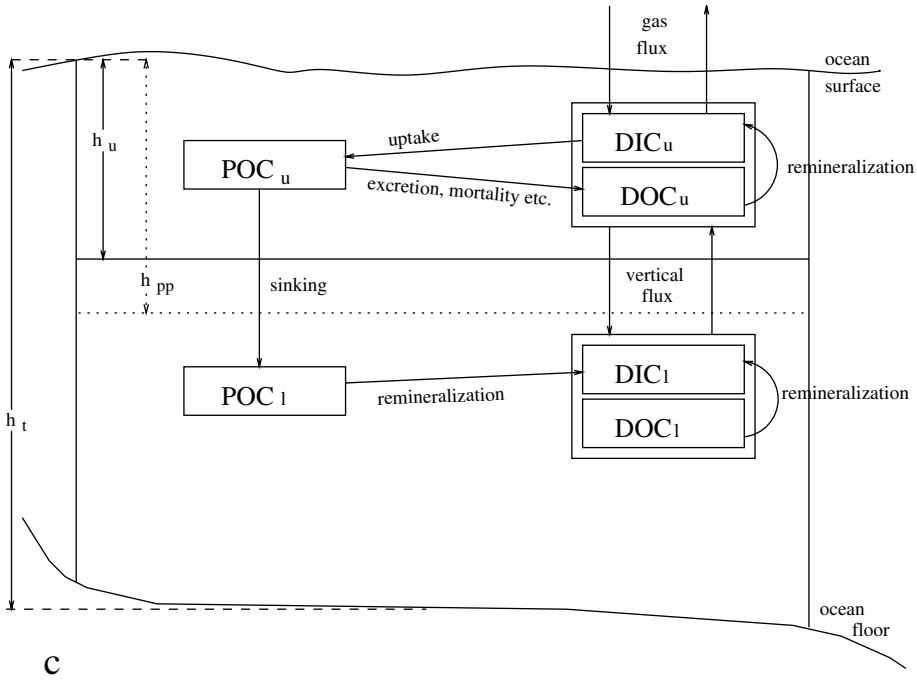

Figure 1. (continued)

ocean through the lower layers of the slope and shelf and then into the surface layer over the shelf. Our shelf box does not include that part of the inner shelf which is landward of the upwelling center. When there are important inputs from the inner shelf, these are modeled as a mixing process (see section 3.3). The model equivalent of the upwelling front is the offshore edge of the slope box. The extent of advection between the coast and open ocean through the front is unknown [*Smith*, 1994; *Mackas and Yelland*, 1999]. In our model the full upwelled volume is advected through the front, recognizing that a portion of it may be advected in the alongshore current. Although downwelling is actually a depression of the pycnocline at the coast, salinities are reproduced reasonably well when representing it by advection (the reverse of upwelling). Alongshore flow is strong in coastal upwelling systems [*Smith*, 1994] but not necessarily the gradients. We assume that these gradients are small (with the exception of the inner shelf buoyancy current, discussed in section 3.3); thus alongshore advection is not modelled. Thisl assumption may be incorrect at times; however, it provides us with a starting point for this modeling exercise.

2.3.2. Entrainment and mixing. [16] The upper layer depth (h_u) is the mixed layer depth which varies seasonally. When h_u changes with time t, entrainment e occurs into the layer, which becomes thicker. It is unrealistic to entrain or mix averaged lower layer concentrations into the upper layer because density profiles do not conform to a perfect two-layer structure, particularly in late summer and early fall. Instead, there is some gradient structure between the bottom of the mixed layer and the nearly homogeneous lower layer. We approximated this structure by modeling a permanent pycnocline (h_{pp}) (different for each horizontal region and fixed in time) with a linear density gradient from it to the bottom of the upper box (Figure 1b), ensuring that $h_u < h_{pp}$ (equation (A5)). The upper box and the region below the pycnocline have uniform concentrations.

Table 1. State Variables for Each Currency[a]

State Variable	Description
DIC	dissolved inorganic carbon
DIN	dissolved inorganic nitrogen
DOC	dissolved organic carbon
DON	dissolved organic nitrogen
POC	particulate organic carbon
PON	particulate organic nitrogen

[a] Units are μM.

2.4. Biological Model

[17] The biological model is a two-layer system. State variables are related to one another by biological fluxes (Figure 1c, (A1), and parameters in Table 3). In addition, dissolved state variables (DI, DO, and S) are exchanged between levels by mixing and entrainment (Figure 1c) as well as by advection (Figure 1a). PO matter can only sink into the lower layer (or be advected between levels). This system was embedded into each of the horizontal shelf and slope regions in the physical circulation model described above. Biological source-sink processes were not modeled in the open ocean system. Open ocean state variable concentrations were specified using data (described in section 3.5).

[18] We model the living PO pool as temperate diatoms, which dominate primary production in coastal upwelling systems where there are large fluxes of nutrients into the euphotic zone [*Hutchings et al.*, 1994]. Diatoms have high growth rates, and their populations often crash suddenly when nutrients become limiting. Sinking rates of single cells can be high (up to 10 m d^{-1} in rare cases) and an order of magnitude higher when cells coagulate and become marine snow [*Smetacek*, 1985; *Alldredge and Silver*, 1988]. Values of the f ratio [*Dugdale and Goering*, 1967] are high [*Harrison et al.*, 1987].

[19] Inorganic nutrients are taken up by the surface (living) PO pool, which is the modeled primary production (PP) via Michaelis Menton kinetics [e.g., *Wroblewski*, 1977]. This uptake is limited by light and the nutrient nitrogen such that only one factor is limiting at any one time. Light-limited photosynthetic rates are determined from an exponential saturation curve (γ) [e.g., *Denman and Peña*, 1999], which is vertically integrated over the upper layer. (There is

Table 2. Physical Parameters and Geometry With Values Used in the Model Runs[a]

Parameter	Description	Value	Units
$\overline{A}$	average upwelling velocity	0.785	m d^{-1}
t_u	upwelling season length	145	d
C	flux per length along coast from VICC	(0.009–0.082)	m d^{-1}
$\overline{D}$	average downwelling velocity: typical, ENSO	0.7, 2.8	m d^{-1}
t_d	downwelling season length	65	d
M_H	horizontal mixing	20	m d^{-1}
M_V	vertical mixing	0.2	m d^{-1}
P	precipitation	(0.002–0.013)	m d^{-1}
R	flux per length along coast from terrigenous runoff	(0.003–0.024)	m d^{-1}
d_m	depth of mixing below h_u	2	m
e_l	entertainment to the lower layer	(−0.007–0)	d^{-1}
e_u	entertainment to the upper layer	(0–0.555)	d^{-1}
h_{pp}	permanent pycnocline: shelf, slope	73, 43	m
H_t	total depth: shelf, slope	120, 400	m
h_u	depth of upper layer: shelf	(10–40)	m
	depth of upper layer: slope	(15–70)	m
w_{sh}	shelf width	20	km
w_{sl}	slope width	10	km

[a] Values in parenthesis were calculated from time dependent functions within the model. Ranges show seasonal variation.

no primary production below the upper layer.) Light is absorbed exponentially with depth by both water and phytoplankton (i.e., self-shading) [e.g., *Fasham*, 1995].

[20] During winter, modeled PP was higher than expected even though integrated light levels were realistic. Since many diatoms go into nonsinking resting stages when growth conditions are not favorable [*Garrison*, 1984], we chose to make part of the surface PO pool dormant during the winter months (equation (A2)).

2.4.1. Excess carbon uptake. [21] In the model, additional uptake of DIC (PC) can occur when DIN is limiting but light is not:

$$\mathrm{PC} = \mathrm{chl}_r(v_m p_0 \overline{\gamma} - \mathrm{PP}) , \qquad (1)$$

where chl_r is a factor to account for the reduction of cellular chlorophyll (chl) relative to carbon, v_m is the maximum nutrient uptake, and $\overline{\gamma}$ is the light limitation function averaged over the upper layer. Variable uptake ratios of DIC:DIN that are greater than the Redfield ratio [*Redfield et al.*, 1963] have been observed in the ocean [*Sambrotto et al.*, 1993]. In an attempt to model this excess uptake we assume that phytoplankton still respond to light and process carbon regardless of nutrient limitation but with an increased C:chl ratio. In the absence of DIN, however, carbon is not incorporated into the cell. Live phytoplankton maintain a C:N ratio in a narrow range close to the Redfield ratio, while C:chl (likewise N:chl) ratios vary widely and are highest when nutrients are limiting but light is not [*Sakshaug et al.*, 1989; *Taylor et al.*, 1997]. Measured DOC:DON ratios are usually well above (7 < DOC:DON > 20) POC:PON (Redfield) ratios [*Hill and Wheeler*, 2002; C. S. Wong, unpublished data, 1997]. Thus we model the excess carbon uptake as passing directly into the DOC pool ((A1a) and (A1c)).

[22] Loss from the living (upper) PO pool is first-order decay (equation (A1b)). The decay rate $s$is scaled by a dimensionless loss function dependent on either nutrient or light limitation (equation (A3)). The numerical coefficients (in (A3)) were chosen so that model equivalent sinking rates ($s\beta ph_u$) are in the range of diatom single-cell sinking rates under nutrient and

Table 3. Biological Parameters and Values Used for Model Runs[a]

Parameter	Description	Value	Units
I_0	daily averaged I_{PAR} at the surface	47–301	W m^{-2}
I_{PAR}	photosynthetically available radiation		W m^{-2}
I_{SAt}	light intensity at which v_m is reached	50	W m^{-2}
K_n	half saturation constant for nitrogen uptake	0.1	μM
K_{sl}	half saturation constant for PO decay due to light limitation	0.06	...
K_{sn}	half saturation constant for PO decay due to N limitation	0.1	μM
α	slope of v_m versus I_{PAR} curve at I_{PAR} = 0	(0.028–0.04)	d^{-}(W m^{-2})
chl_r	chlorophyl reduction factor	0.2	...
k_p	I_{PAR} attenuation coefficient for PON	0.06	m^{-1}(μMN)
k_w	I_{PAR} attenuation coefficient for seawater	0.04	m^{-1}
p	fraction of particulate flux leaving PO_u pool	0.6	...
p_0	active surface PO concentration (C or N)		μM
pc	excess carbon uptake		μM C d
pp	primary production (C or N)		μM d^{-1}
r_d	dissolved organic matter decay rate: C, N	0.005, 0.0065	d^{-1}
r_p	particulate organic matter decay rate	0.2	d^{-1}
s	decay rate of surface PO pool	0.0385	d^{-1}
v_m	maximum growth rate for phytoplankton	(1.4–2.0)	d^{-1}
v_{m0}	maximum growth rate for phytoplankton at 0 K	5.696×10^{-9}	d^{-1}
γ	$1-\exp(-\alpha I_{\mathrm{PAR}}(z/vm)$	0–1	...

[a] See Appendix D. Values in parenthesis are results of model conclusions. Ranges show seasonal variation.

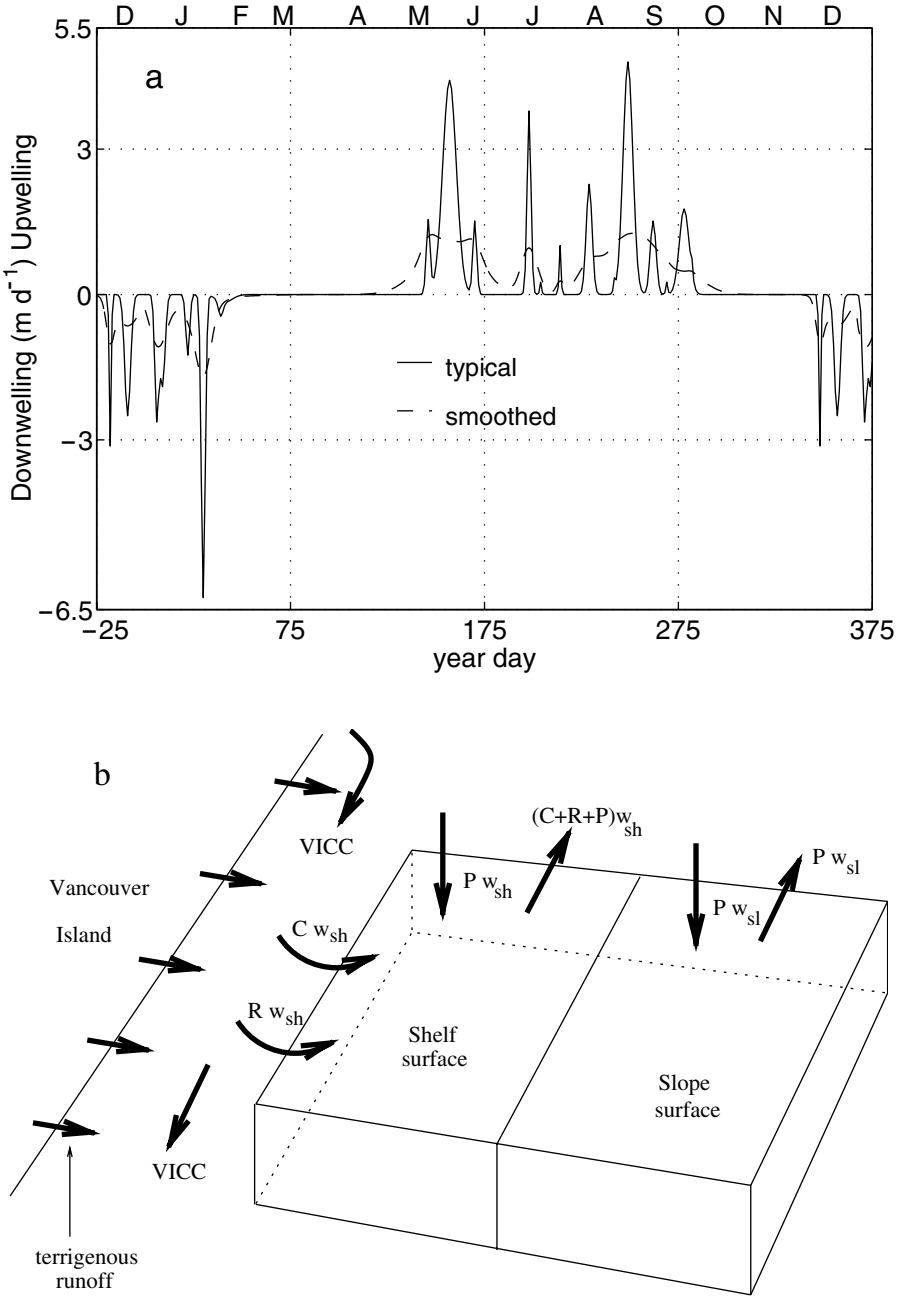

Figure 2. (a) A typical year of realistic external forcing. Positive values are A during the upwelling season and negative values are D during the downwelling season. The dashed curve shows smoothed forcing for the same integrated flux as the typical year. (b) A schematic of the upper layer shelf and slope boxes showing buoyancy fluxes. Buoyancy fluxes (volume per length coastline) from precipitation are Pw_{sh} and Pw_{sl}. Buoyancy fluxes (volume per length coastline) from the inner shelf are from terrigenous runoff (Rw_{sh}) and from the VICC (Cw_{sh}).

light limitation, respectively [*Bienfang et al.*, 1982, 1983]. The total decay flux is partitioned between the lower PO and upper DO pools ((A1e)) and (A1c)), so that the fraction p goes into the lower PO pool. In a one-dimensional system in steady state, p is a first-order approximation of the f ratio, as all particulate flux sinks immediately to the lower box while the dissolved portion stays in the surface. Transfers between trophic levels are not modeled. Nonliving organic matter (DO and lower PO pools) remineralizes ((A1c), (A1f), and (A1e)) to DI pools ((A1a) and (A1d)) via first-order exponential decay at their respective decay rates (r_d, r_p), which are different for each currency.

2.5. Gas Flux

[23] The surface partial pressure of CO_2 (pCO_{2w}) was calculated from modeled DIC and alkalinity (ALK) using the relationships of *Skirrow* [1975], prescribed sea surface temperatures T, and modeled S. The sea surface salinities are fresher than the averaged box value, so they were extrapolated by subtracting ΔS from S_u. Model DIC was diluted by the same amount to

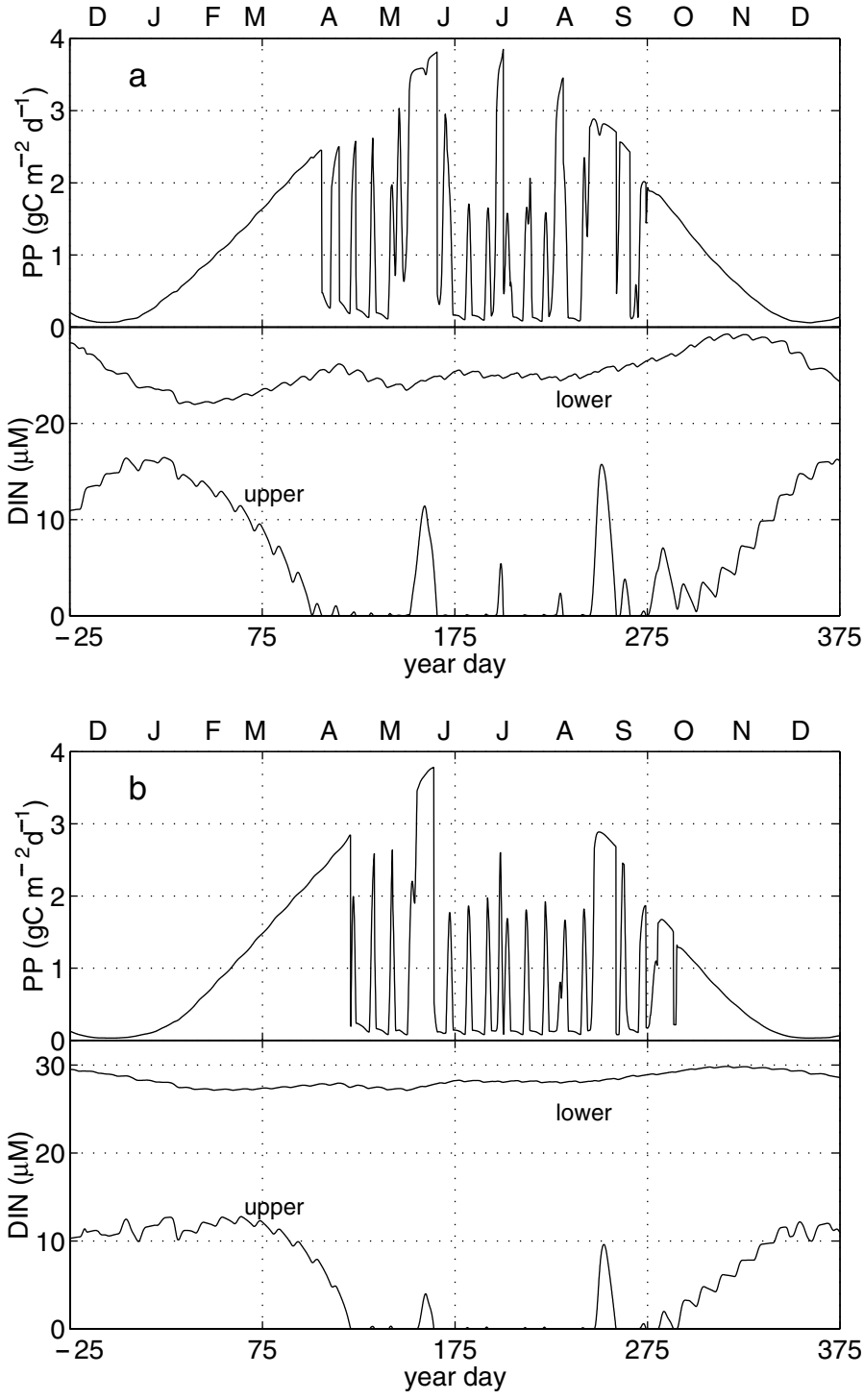

Figure 3. (a) Integrated shelf and (b) slope primary production (top panel) and upper and lower layer shelf DIN (bottom panel) for a typical year. Advective forcing is shown in Figure 2a. The modulating wave in DIN is caused by entrainment in response to storm forcing. Time is in year days, where year day 0 is 1 January.

determine surface DIC. The model assumes that dilution exerts the major control over ALK (based on summer measurements in the study area [*Ianson*, 2001]); thus calcium carbonate ($CaCO_3$) formation is not modeled. We use a linear relation between the measured ALK and salinity (ALK = 52.85 S + 472 μeq kg^{-1}; r^2 = 0.80) [*Ianson*, 2001] to estimate model ALK. The single negative charge associated with modeled DIN (assuming that the bulk of the DIN is nitrate) was then subtracted to estimate carbonate ALK. Annual variability of atmospheric pCO_{2a} was prescribed [*Manning*, 1993]. Gas flux $G$was determined from the solubility of CO_2, piston velocity k, and the pCO_2 of water and air using the standard equation [e.g., *Watson*, 1993]. Solubility

Table 4. Comparison of Annual Gas Flux $(\overline{G})$, Annual PP $(\overline{PP})$, and Nitrogen Inventory $(\overline{N_i})$ for Different Model Runs[a]

Run	Description	Winter Shelf $\overline{pCO_2}$, ppm	Summer Shelf $\overline{pCO_2}$, ppm	Total $\overline{G}$, g C $m^{-2}yr^{-1}$	Total $\Delta\overline{PP}$, %	Total $\Delta\overline{N_i}$, %
1	typical	505	230	6	0	0
2	α increased 35%	470	230	19	10	2
3	smooth forcing	530	230	3	20	6
4	$\overline{A}t_u:\overline{D}t_d = 3.2$	530	230	1	2–3	6
5	$p = 0.3$	470	230	14	−10[b]	−6[b]
6	r_d is doubled	540	230	−1	5	<6[b]
7	$\overline{A} = \overline{D} = 0$	450	270	14	−50	−25
8	ENSO[c]	435	230	22	−20[c]	−12[c]
9	PC = 0	505	310	0.6	0	0

[a] Positive $\overline{G}$ is invasion. Shelf pCO_2 were averaged over January to represent maximum winter values and over June and July to represent minimum summer values. $\overline{G}$, $\Delta\overline{PP}$ and $\Delta\overline{N_i}$ were calculated by weighting annual flux over the shelf by two relative to the slope to account for its larger area. $\Delta\overline{PP}$ and ΔN_i were determined relative to run 1.

[b] These differences are relative to a run with $p = 0.7$ rather than $p = 0.6$ (run 1). (All other parameters are from run 1.)

[c] Note that the ENSO year follows a typically forced year, while forcing is the same each year in other runs. When ENSO years repeat, differences (with respect to run 1) increase.

was estimated from S and T using the relationship of *Weiss* [1974]. The relationship of *Wanninkhof* [1992] for k based on long-term averaged wind was used.

3. Physical Forcing

[24] The external physical forcing makes the model specific to a particular coastal upwelling region. We present results for the west coast of Vancouver Island, Canada. Upwelling and downwelling circulation, light, mixed layer depth, and buoyancy fluxes are all forced by external functions based on local data and are described below.

3.1. Upwelling and Downwelling

[25] The upwelling index of *Thomson and Ware* [1996] was used to specify the average timing of the seasons as well as the frequency and relative strength of upwelling and downwelling events. The average of the absolute upwelling and downwelling strength was based on field estimates [*Freeland and Denman*, 1982; *Freeland and McIntosh*, 1989]. A smoothed version of this forcing function with the same averaged velocities and seasonal timing was also used to compare the effects of smooth versus realistic forcing (Figure 2a). Forcing during El Niño-Southern Oscillation (ENSO) years was based on *Hsieh et al.* [1995], who showed that during a typical ENSO year in our study area, downwelling strength is enhanced while upwelling strength remains constant.

3.2. Light, Wind, Temperature, and Salinity

[26] Sea surface measurements of I_{PAR} (D. Crawford, personal communication, 1997; S. Harris, unpublished data, 1998) set the annual light cycle. The Pacific Northwest experiences thick cloud cover during a large part of the year, so light availability is often low. Wind data [*Faucher et al.*, 1999] were averaged over the seasons to calculate the piston velocity. A typical seasonal cycle in temperature was prescribed (http://www.ios.bc.ca/ios/osap/data/lighthouse/bcsop.htm; R. Brown, unpublished data, 1998). The amount of surface freshening, ΔS, relative to the average box value for shelf and slope was 0.2 and 0.03, respectively (R. Brown, unpublished data, 1998).

3.3. Buoyancy Flux

[27] Coastal freshwater additions are important to our model as they dilute both DIC and alkalinity and so have a major impact on pCO_2. The west coast of Vancouver Island experiences ~3 m yr^{-1} of rain (British Columbia Department of Agriculture (Victoria, British Columbia, Canada), Climatic normals 1941–1970), most of which falls in the late fall and early winter. Buoyancy flux is added to the model via rainfall P over both the shelf and slope and also as terrigenous runoff R into the shelf box (Figure 2b and Appendix B).

[28] A buoyancy current, the Vancouver Island Coastal Current (VICC), flows northward year-round over the inner shelf [*Freeland et al.*, 1984] and provides a large flux of DIN [*Pawlowicz*, 2001], although gradients of other state variables are assumed small [*Ianson*, 2001; C. S. Wong, unpublished data, 1997]. The VICC is modeled like runoff as a scaled flux into the surface shelf box (Appendix B). The additional volume added to the shelf and slope surface boxes exits the system in the alongshore current (Figure 2b).

3.4. Mixed Layer Depth

[29] The depth of the upper box h_u is the mixed layer depth. The annual cycle in mixed layer depth was prescribed using the results of Thomson and Fine (personal communication, 1999) with additional variability at storm frequencies added (Appendix C).

3.5. Open Ocean

[30] Seasonal variations in all surface ocean state variable concentrations were forced, while deep ocean concentrations were held constant [*Ianson*, 2001] based on the data of *Whitney et al.* [1998], *Wong et al.* [1997], *Bishop et al.* [1999], *Whitney and Freeland* [1999], C. S. Wong (unpublished data, 1997), and R. Brown (unpublished data, 1998).

4. Results

4.1. Primary Production

[31] The response to the typical upwelling and downwelling forcing (Figure 2a) by DIN and primary production presented over the shelf and over the slope (Figure 3, run 1) shows a gradual increase in PP in response to increased light availibility (in the sense of *Sverdrup*[1953]) followed by an abrupt crash when DIN in the upper layer becomes depleted (occurring later over the slope). Storm mixing and entrainment provide DIN for small bursts of primary production until the upwelling season begins (year day 145). Upwelled fluxes into the upper layer are large so that upper layer DIN builds up faster than the biota can draw it down, so sharp peaks in DIN and PP over the shelf occur (Figure 3a). Much of the

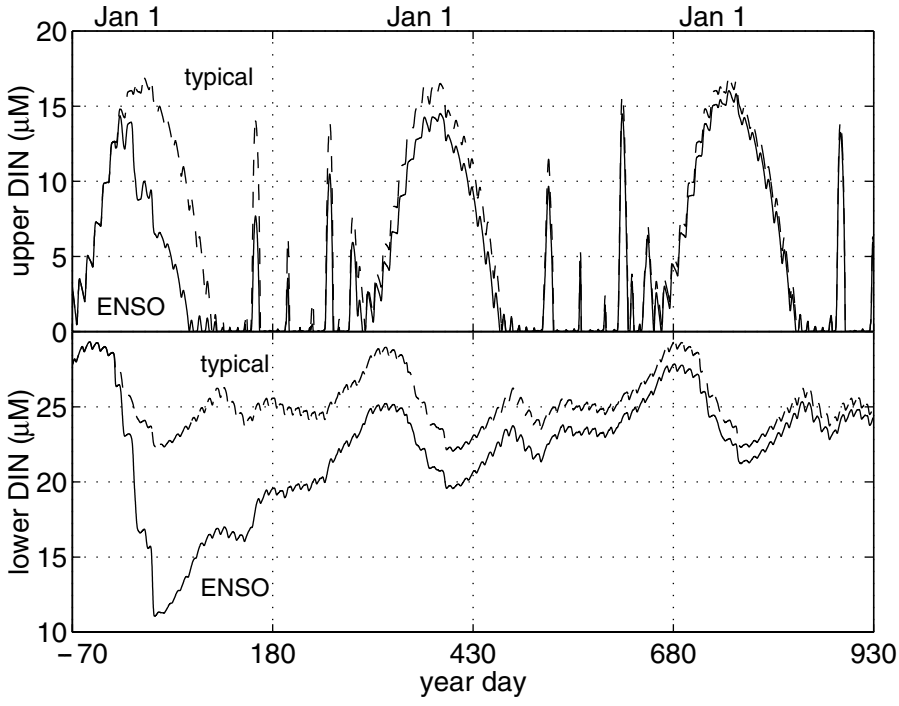

Figure 4. Shelf DIN in upper layer (top panel) and shelf DIN in lower layer (bottom panel) for 3 years. ENSO response (solid curve) to ENSO forcing during the first year (followed by typical forcing in the second and third year) is compared to 3 years of typical forcing (dashed curve).

upwelled DIN is taken up over the shelf before it can be advected offshore into the upper slope box. Thus, over the slope these peaks are much smaller and only occur for large upwelling events (Figure 3b). In the fall, DIN increases in the surface mainly due to entrainment and reduced demand because of decreasing light availability. In the lower shelf layer (Figure 3a, bottom panel), DIN decreases as the nutricline becomes depressed during the short winter downwelling season (year days 349–45), but DIN increases throughout the upwelling season (year days 145–285) due both to advection from the open ocean and remineralization. DIN in the lower slope box (Figure 3b, bottom panel) behaves similarly but with less variation throughout the year. Net annual primary production for the typically forced case is 410 and 330 g C $m^{-2}yr^{-1}$ for the shelf and slope, respectively. Model PP is higher than previously expected (around 250 g C $m^{-2}yr^{-1}$ from local observations (P. Harrison, personal communication, 1997)) but is in agreement with recent measurements [*Ianson*, 2001; S. Harris, unpublished data, 1998].

[32] In the surface shelf box, DIN supplied by upwelling is responsible for 50% of PP, while mixing and entrainment provides 35% and the VICC provides 15%. Over the inner shelf, which we do not model, the VICC is likely the major nutrient source. Over the slope, upwelled DIN fuels 30–35% of the PP, mixing fuels 65–70%, and the VICC fuels <5%.

[33] Primary production is mainly controlled by light availability in our study area when physical forcing is realistic, i.e., not smoothed in time (Figure 2a). The maximum possible daily PP when nutrients are not limiting is controlled by I_{PAR} through the biological uptake parameters, α (uptake rate per light intensity at low light levels), and to a lesser degree, v_m (maximum uptake rate). When the model PP drops during the summer, it is nutrient limited or briefly light limited through PO matter self-shading. Because I_{PAR} is usually below I_{SAT} throughout the upper layer, the model is not sensitive to changes in v_m. To understand the sensitivity of the model to these and other parameters, additional runs were preformed (Table 4). Increasing v_{m0} by 35% (but maintaining α through a comparable increase in I_{SAT}) has no effect on model PP. At low light levels, α is important. Increasing α by 35% (with v_{m0} constant; run 2) causes PP to increase by 10% as the maximum possible daily PP is higher. However, changing the way that nutrients are delivered to the euphotic zone has a major effect on PP.

[34] When forcing is smoothed (peak width of each event increased by a factor of 4) (Figure 2a) but integrated upwelling and downwelling flux is the same (run 3), primary production increases significantly (by 24%) over the shelf (510 g C m^{-2} yr^{-1}) but decreases (by 15%) over the slope (280 g C m^{-2} yr^{-1}). There is higher primary production in the system because the peak upwelled DIN fluxes are small enough that the biota can respond before the DIN is horizontally advected into the open ocean. In the more sporadic (typical; run 1) case some DIN is advected out of the system during strong events before it can be utilized by the biota. The effect of this higher production (20%) under smooth forcing is to maintain a larger nutrient inventory in the system (~6% in nitrogen) despite the same net advected nitrogen flux into the system. Much of the additional primary production is remineralized over the shelf, and so more nutrients are retained.

[35] Nutrient inventory is clearly influenced by primary production as in the example above. Of the physical parameters, the most important to nutrient inventory are the average upwelling and downwelling velocities ($\overline{A}$ and $\overline{D}$), in particular the ratio of total annual fluxes ($\overline{A}t_u$:$\overline{D}t_d$), where t_u and t_d are the lengths of the upwelling and downwelling seasons, respectively. Horizontal mixing is less important. The higher $\overline{A}t_u$:$\overline{D}t_d$, the higher the nutrient inventory over the shelf. Some of the increased nutrient supply is used in PP. Increasing this ratio to 3.2 ($\overline{A} = 0.865$ and $\overline{D} = 0.6$ with unchanged season durations, t_u and t_d; run 4) from 2.5 (typical value; run 1) causes a 2–3% increase in PP and an increase in total nitrogen inventory by 6%. Also, the nutrient concentration in the lower layer of the neighboring open ocean (the depth of upwelling) is important, as this water is advected onshore each summer.

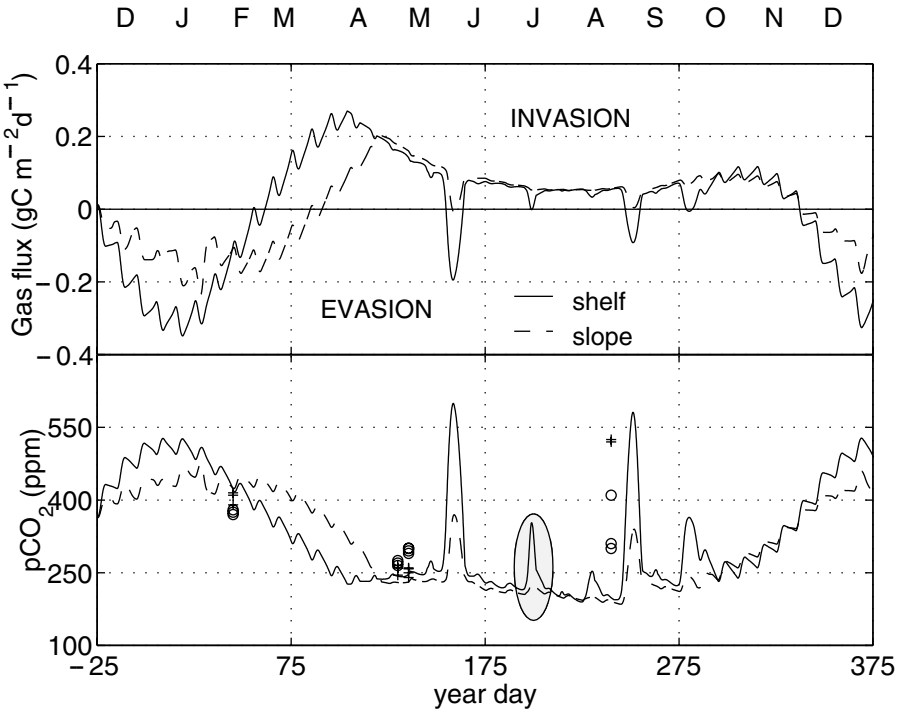

Figure 5. Model gas flux (top panel) and pCO_2 (bottom panel) for shelf (solid curve) and slope (dashed curve). Positive gas flux is from the atmosphere (invasion). Measured pCO_2 in the study area from ship of opportunity cruises (C. S. Wong, unpublished data, 1997) collected September 1995 (during an upwelling event), May 1995 and 1996, and February 1996 over the shelf (pluses) and slope (open circles) and an ellipse of measured pCO_2 [*Ianson*, 2001] collected in July 1998 are shown for comparison with the model. The July 1998 data were collected following an upwelling event and during a relaxation period (i.e., between events) and so cover a range in pCO_2 as shown by the ellipse. (The ellipse is centered on the average of the data (in time and pCO_2) over both shelf and slope.) Note that the model forcing is that of a "typical" year, and so the timing of upwelling events is not the same as in the data.

[36] Increasing the fraction p of the decay flux from the surface PO pool which sinks and becomes PO in the lower layer also increases nutrient inventory (6% with a change in p from 0.3 (run 5) to 0.7) and therefore primary production (10% for the same change). With the higher p, more remineralization occurs over the shelf as the particulate rate r_p is an order of magnitude higher than the dissolved rate r_d. In addition, it occurs in the lower layer, where it is more likely to be retained in the system as most PP occurs during the upwelling season. In the case where p is low, there is higher horizontal export of DO matter out of the system in the surface layer. Doubling the rates of PO remineralization r_p has little effect on either nutrient inventory or PP, as the original rate was high enough that close to complete remineralization already occurred within the system. Doubling the remineralization rates of DO matter r_d (run 6) increases the nutrient inventory only slightly (<1%) but increases total PP by 5% as the excess remineralization occurs mostly in the surface and so is quickly taken up by the biota.

[37] When upwelling and downwelling circulation is shut off completely (run 7), the model behaves more like an oligotrophic ocean. Primary production decreases to half and is nutrient limited during the entire summer. DIN concentrations are lower everywhere in the system. Surface DIN is 30% less in the winter over the shelf and is zero throughout the summer. The total nitrogen inventory decreases by 25%.

4.1.1. ENSO. [38] Simulations of ENSO (run 8) show effects of interannual variability in forcing and that winter forcing can affect the summer season. During ENSO years, modeled downwelling is enhanced, while upwelling remains the same. Despite the same upwelled flux during the summer, primary production is lower (∼20% from increasing $\overline{D}$ from 0.7 to 2.8). The nutrient inventory in the system is decreased because the nutricline is so strongly depressed during the winter that the summer upwelled water has lower DIN (Figure 4). This effect can clearly be seen in the DIN concentration of the lower shelf box (Figure 4, bottom panel) which drops to 11 μM during the ENSO winter. If the nutricline in the open ocean were also depressed or if summer upwelling were decreased, the effects of ENSO would be enhanced. After one winter of increased downwelling, the system takes ∼4 years to reach its previous steady state nutrient inventory (Figure 4), though in the second year after ENSO, primary production is within 5% of its initial value (but less nutrients are advected out of the system). ENSO events occurring at frequencies higher than every 4 years decrease the nutrient inventory and production in the system over the long term.

4.1.2. Residence Time. [39] The residence time for water over the shelf in the model is of the order of weeks in the surface layer (∼10 days in the summer and ∼50 days in the winter) and ∼4 months in the lower layer. These times seem reasonable relative to the natural system; however, the strong alongshore circulation is not modeled and could shorten them substantially depending on the alongshore extent of the model (larger spatial scale, less effect on residence time). In the case of the ENSO example above the spatial extent of the physical forcing is large (order of 1000 km), and so our model results would not be greatly affected by the addition of the alongshore circulation. In addition, residence time

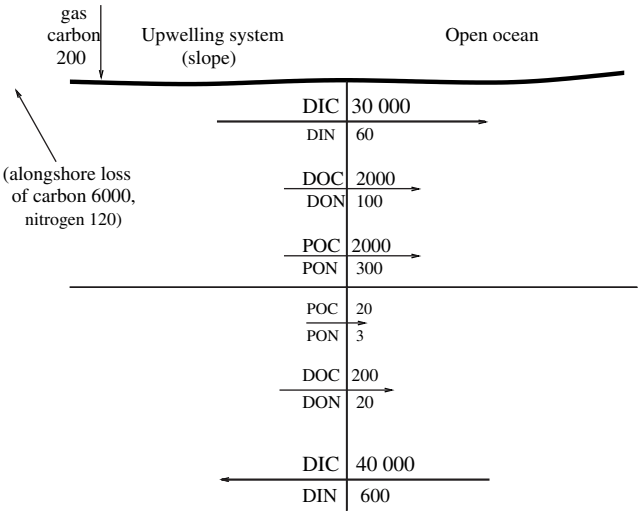

Figure 6. Net annual exchange between the model system and the ocean are shown for each form of carbon and nitrogen. In addition, net alongshore fluxes occur from upper shelf and slope boxes. All units are per length of coastline (in m) (kg yr^{-1} m^{-1}).

for nutrients is longer because nutrients are incorporated into the PO matter, some of which sinks into the lower layer, retaining nutrients in the system.

4.2. Gas Flux

[40] For all model configurations, there is air-sea CO_2 evasion during the winter and invasion during the summer, when PP draws down surface DIC (Figure 5, top panel). However, net annual CO_2 flux is much smaller than these seasonal fluxes. For the typically forced case (run 1; Figure 5), there is net annual invasion (6 g C m^{-2} yr^{-1}, which is 2×10^5 g C yr^{-1} per m coastline) (Table 4). Over the shelf, surface pCO_2 varies over a larger range (200–550 ppm) than over the slope (200–450 ppm), similar to sparse field measurements (Figure 5, bottom panel). The highest model pCO_2 occurs over the shelf in response to strong upwelling events (year days 159 and 251). While these values seem high, surface measurements of 525 ppm have been recorded during an upwelling event in the area (day 240, Figure 5). Between upwelling events, pCO_2 is around 200–250 ppm, which compares with measurements (year days 195–205, Figure 5, discussed by *Ianson* [2001]). In the winter model, pCO_2 is high due to low alkalinity (from high rainfall) and increased DIC (from vertical mixing) in agreement with data (day 45, Figure 5). The pCO_2 is highest over the shelf, where the surface waters are freshest. Primary production draws pCO_2 down earlier in the spring over the shelf than over the slope (Figure 5, days 100–125 in the model, day 130 in the data), but otherwise, the model output is similar for both.

[41] Sensitivity studies show that variations in model parameters do affect pCO_2; however, summer pCO_2 is remarkably insensitive as long as upwelling and downwelling circulation are not set to zero. Only large changes in assumed deep ocean DIC concentration or setting excess carbon uptake (PC) to zero (run 9) cause summer pCO_2 to vary from the typically forced case. Most variations appear during the winter season even for differing PP.

[42] Increasing carbon inventories (by either using smoothed forcing (run 3) with the same $\overline{A}t_u:\overline{D}t_d$ ratio or by increasing $\overline{A}t_u:\overline{D}t_d$ to 3.2 (run 4) with realistic forcing) causes winter and fall pCO_2 to increase by 20–30 ppm, while summer values are unchanged. There is still net annual CO_2 invasion, but it is significantly decreased (Table 4). There is higher invasion in the smoothed case because there are no high pCO_2 peaks in summer from upwelling. Doubling the remineralization rate of DOC (r_d) (run 6) does not change summer pCO_2 but increases fall and winter pCO_2 by ~50 ppm. Decreasing nutrient inventory by lowering $p$to 0.3 (run 5) makes for lower winter pCO_2 (by 40 ppm), increasing the net gas invasion (Table 4).

[43] Winter pCO_2 is lowered in the case of ENSO forcing (enhanced downwelling; run 8). The depression of the pycnocline and the concentration decrease of DIC is strong, and so winter pCO_2 decreases by ~70–80 ppm, while summer values remain the same (Table 4). Winter and spring pCO_2 are lowered (40–50 ppm) when PP is increased (10%) by increasing the biological parameter α (35%; run 2) while summer values remain unchanged despite higher daily PP. In both the above examples, there is larger net annual CO_2 invasion (~20 g C m^{-2} yr^{-1}).

[44] When there is no excess DIC uptake by the surface PO pool (run 9), pCO_2 is significantly higher, as much as 80–90 ppm, during the summer (Table 4). The carbon inventory does not change though, so winter pCO_2 is not affected. Net annual gas invasion decreases relative to the typical case to near zero. In this scenario, however, model DIC between upwelling events is higher than measured [*Ianson*, 2001] (Figure 5).

[45] Shutting off the upwelling and downwelling circulation entirely (run 7) causes a 40 ppm increase in summer pCO_2 as PP is reduced by about half. Net annual CO_2 invasion still increases (by a factor of 2) because of decreases in winter and fall pCO_2. With no upwelling circulation, nutrient inventories are significantly less (because primary production is lower and also because DIC is not advected into the system during summer), causing fall and winter DIC concentrations to be lower. A much larger portion of the summer DIC drawdown in this scenario, however, is due to PC. If it were not for this excess uptake of carbon, there would be close to zero net annual CO_2 flux.

4.3. Net Annual Exchange Fluxes Between the Model and the Open Ocean

[46] For both carbon and nitrogen the dominant annual exchange flux is the import flux of DI nutrients into the lower slope box from the open ocean (Figure 6). This nitrogen input is balanced mainly by export of PON from the upper layer to the surface open ocean (50%). Lower layer exports of PON are small, two orders of magnitude less than surface exports. A further 20% of the DIN import is exported to the open ocean as DON, mainly in the upper layer (Figure 6), while 10% leaves as DIN in the upper layer. The remaining 20% leaves the system in the alongshore surface current as a result of the buoyancy fluxes. While there is a net import of DIN from the VICC, a much larger alongshore export occurs as DON and PON.

[47] In the case of carbon, most (75%) of the lower layer DIC import flux returns to the open ocean as DIC in the upper layer (Figure 6) because the fraction of biological DIC drawdown is so much smaller than that of DIN. Only 10% of the carbon import leaves as organic carbon in the surface layer in equal fractions of DOC and POC. Fifteen percent of the imported DIC is exported in the alongshore surface current due to buoyancy fluxes, mostly as DIC over the shelf. Although gas flux provides an additional net import of carbon, it is two orders of magnitude less than the lower layer import of DIC.

[48] The C:N ratio of the PO export is 6.7 (set in the model), while the C:N ratio of the model DO export is in the range of 10–20. The ratio of total TOC:TON export is ~10, which agrees

well with depth-integrated measurements in the upwelling region along the Oregon coast (44.65°N, 124.18°W) [*Hill and Wheeler*, 2002].

[49] Sensitivity studies show that when upwelling strength is increased relative to downwelling strength ($\overline{At_u}$:$\overline{Dt_d}$ = 3.2 run 4), both lower layer DI imports increase by 20%. Almost all of the excess DIC import is exported into the surface ocean as DIC. About half of the excess DIN leaves in the surface as DIN, while the other half is converted to organic nitrogen, which is then exported into the surface ocean. When PP is increased through smooth forcing (run 3), DIC exchanges are unchanged, but there is no longer any DIN export in the upper layer. There is a shift (factor of 2) in organic matter export in the surface from POC to DOC. Likewise, increasing PP (10%) by raising α (run 2) does not affect DIC exchange while DIN export to the surface ocean is much lower (60%). Organic matter exports increase in both layers by 10–20%.

[50] If upwelling and downwelling circulation is shut off (run 7), exchange fluxes with the open ocean decrease by an order of magnitude. Import of DIC still occurs in the lower layer, but it is balanced mainly by the export of DOC rather than DIC in the upper layer.

5. Discussion

[51] Results show that the winter season is very important in determining model fluxes, despite the fact that the major biological fluxes occur during the summer. Downwelling strength has a major impact on lower layer nutrient concentrations over the shelf and in turn PP the following summer. Interannual variability (such as ENSO events) affects the system over timescales of 3–5 years. Furthermore, it is differences in winter (not summer) surface pCO_2 that cause differences in modeled net annual CO_2 flux. During the winter the lower layer is thoroughly mixed and entrained into the surface layer over the shelf. Because of this winter mixing, nutrient inventories in the system have a strong influence on both PP and pCO_2. The primary influences on nutrient inventory are the ratio of upwelling and downwelling strengths, PP, and p (mainly because more organic matter is remineralized at a higher rate when p is increased). In addition, the nature of advective forcing is important. Realistic and more sporadic forcing versus smoothed forcing (Figure 2a) yields significantly lower PP (20%) and nutrient inventory (6%). Freshwater inputs during winter also exert strong control over pCO_2 by lowering ALK.

[52] To develop this model, we made several additions which are nonstandard relative to the biological models reviewed by *Fasham* [1993]. These additions were necessary to produce reasonable results. Physically, a permanent pycnocline was added to create more realistic vertical variability in state variables (Figure 1b). Without this variability, entrained and mixed fluxes were too large, particularly during late summer and fall. Entraining-averaged lower layer DIN at these times made fall surface DIN unrealistically high and produced a large fall phytoplankton bloom (comparable to upwelling blooms). Biologically, winter PP was too high (>0.3 g C $m^{-2}d^{-1}$) despite realistic light levels. High PP during the winter meant that surface nutrients did not attain measured spring values, and the resultant spring bloom was much smaller than expected. To solve this problem, we made a portion of the living PO pool dormant during the winter months (equation (A2)) representing the formation of nonsinking resting stages by diatoms. We also modeled excess uptake of DIC during times of nutrient limitation (1) so that summer surface DIC values reflected measured values. This excess flux was added to the DOC pool, thereby increasing the model TOC:TON ratio from the Redfield ratio to a more realistic value of ~10. Raising the DON remineralization rate relative to that of DOC also raises the TOC:TON ratio. In addition, our characterization of nonliving organic matter as sinking (PO) or nonsinking (DO) is unique. Because the living PO pool maintained quite large concentrations even when nitrogen and light became limiting, we made the decay rate of this pool increase at these times. We based increased losses on changes in phytoplankton single-cell sinking rates. This representation produced better results than a mathematical representation of zooplankton grazing [*Ianson*, 2001].

[53] The model parameters which are most important to predict the system are the offshore lower layer inorganic nutrient concentrations, α (particularly at middle to high latitudes), p, and r_d. The former is generally known, while the three latter parameters are not as well known. The most poorly known are p and r_d, which determine the character of the nonliving organic matter, whether sinking or nonsinking, and the remineralization rates.

[54] The model is limited to decadal timescales because important processes (over longer timescales) such as denitrification and sedimentation are not modeled. In locations where $CaCO_3$ formation occurs, it would be necessary to incorporate this cycle to model pCO_2 (due to the reduction of surface ALK [*Broecker and Peng*, 1982]). In addition, if N_2 fixation occurs in the study area, it could have a major impact on the ecosystem dynamics; however, there is currently no evidence for it in our study area.

[55] Our model was developed to be general and could easily be extended to other upwelling regions. What makes the model area specific is the physical forcing. Most important are quantification of the advective circulation and exchange with the complex inner shelf (buoyancy fluxes). In addition, the open ocean concentrations of inorganic state variables are crucial to the model, and reliable seasonal data are needed for two state variables (in our case, S and DIN) to tune the physical model. In other upwelling regions, riverine input of DO matter and stronger upwelling circulation would be interesting to investigate and would provide different outcomes. However, many upwelling regions do not experience the downwelling season as in our study area, and so our results of large net flux of DIC into the surface ocean would be enhanced, as would the importance of winter mixing and gas evasion.

[56] It is difficult to calculate CO_2 gas flux accurately, so we do not pretend that the results of our simple model yield firm numbers. Our model does indicate the chief influences on gas flux and shows that within the system, winter evasion is of the same order as summer invasion (so the net flux is relatively small) in all model runs. This net flux is usually into the ocean even when the parameters are stretched to their limits (the exception is the doubling of r_d, which causes small evasion).

6. Conclusions

[57] The model suggests that the largest influence on the global carbon budget from coastal upwelling regions is ventilating intermediate depth oceanic DIC through large imports of DIC into the lower layer of the system, most of which exits back to the open ocean in the surface layer. Furthermore, this advected surface flux is relatively deplete in DIN. High PP over the shelf does not make for strong biological pumping; rather, it creates high nutrient inventories that are mixed into the surface (where DIC is ventilated) during winter. Organic matter is also horizontally exported into the open ocean but mostly in the upper layer. There is little export of organic matter in the lower layer (over an

order of magnitude less). The surface organic carbon export is split roughly equally into DO and PO, so that some of it may sink in the open ocean but most of it is likely to be remineralized in the surface. Thus, while coastal upwelling regions have disproportionately high PP and pCO_2 drawdown, they are unlikely to absorb atmospheric carbon via the biological pump. The dynamic physical processes in winter ventilate the DIC, which accumulates in the lower layer during the summer, and the advective circulation transports large quantities of intermediate depth ocean water, rich in DIC, to the surface.

Appendix A. Model Equations

A1. Biological Model

[58] Using carbon as a currency, the general ordinary differential equations for the upper layer are

$$\frac{d\mathrm{DIC_u}}{dt} = -\mathrm{PP} - \mathrm{PC} + r_d\,\mathrm{DOC}_u + \frac{G}{h_u} + V + X + H \tag{A1a}$$

$$\frac{d\,\mathrm{POC_u}}{dt} = \mathrm{PP} - (s\,\mathrm{POC}_u\beta) + X + H \tag{A1b}$$

$$\frac{d\mathrm{DOC}_u}{dt} = [(1-p)\,s\,\mathrm{POC}_u\beta] + \mathrm{PC} - r_d\,\mathrm{DOC}_u + V + X + H, \tag{A1c}$$

where PP is primary production, r_d is the DOC remineralization rate, G is the gas flux, and PC is excess carbon uptake (described in text). Physical terms are represented by V (vertical mixing and entrainment), X (advection), and H (horizontal mixing) and are defined below. In (A1b) the second term on the left-hand side is the decay of the upper (living) POC pool, where s is the decay rate and β is a dimensionless function dependent on growth conditions (equation (A3)). The fraction of this decay flux that sinks into the lower layer as particulate flux is p. In the lower layer,

$$\frac{d\,\mathrm{DIC}_l}{dt} = r_d\,\mathrm{DOC}_l + r_p\,\mathrm{POC}_l + V + X + H \tag{A1d}$$

$$\frac{d\,\mathrm{POC_l}}{dt} = \frac{sph_u\beta}{h_t - h_u}\mathrm{POC}_u - r_p\,\mathrm{POC}_l + X + H \tag{A1e}$$

$$\frac{d\,\mathrm{DOC}_l}{dt} = -r_d\,\mathrm{DOC}_l + V + X + H\,, \tag{A1f}$$

where r_p is the POC remineralization rate. The fraction of the of the POC (p_o) which is active (i.e., takes up nutrients in PP) is

$$p_0 = \mathrm{PO}\left\{1 - \exp\left[-0.1\ \mathrm{W^{-1}m2(I_0(noon)-43\ Wm^{-2})}\right]\right\}\,, \tag{A2}$$

where I_0(noon) is I_{PAR} at midday. The loss function is

$$\beta = \mathrm{MAX}\left(9 - \left(8\frac{\mathrm{DIN}}{\mathrm{DIN} + K_{sn}^2}\right),\ 6 - \left(5\frac{\overline{\gamma}^2}{\overline{\gamma}^2 + K_{sl}^2}\right)\right), \tag{A3}$$

where K_{sn} is the half saturation constant for PO decay due to nitrogen limitation and K_{sl} is that for light limitation. Values of biological parameters are shown in Table 3. Fluxes are described in the text and illustrated in Figure 1c. The equations are identical for nitrogen, except that there is no gas flux or excess uptake (PC), while for salinity, there are only physical terms.

A2. Physical Terms

[59] The physical terms in the model equations $V(q)$, $H(q)$, and $X(q)$ represent vertical mixing, horizontal mixing, and advection, respectively, for the state variable q. The indices i and j represent horizontal (sh, sl, and o) and vertical (u and l) dimensions, respectively. Note that $(i-1)$ is the horizontal region immediately inshore of i and similarly $(i+1)$ is the horizontal region immediately offshore of i.

$$V_{i,j}(q) = \left(\frac{M_v d_m}{h_{i,j}\left(h_{i,pp} - h_{i,u}\right)_i} + e_{i,j}\right)\left(q_{i,k} - q_{i,j}\right)\,, \tag{A4}$$

where $k = \ell$ if $j = u$ and vice versa. The entrainment rates ($\mathrm{e}_{i,\,j}$) are

$$e_{i,u} = \mathrm{MAX}\left(\frac{dh_{i,u}}{dt}\left(h_{i,pp} + h_{i,u}\right)^{-1}\quad,\quad 0\right) \tag{A5a}$$

$$e_{i,l} = \mathrm{MIN}\left(\frac{dh_{i,u}}{dt}\left(2h_{i,t} - h_{i,pp} - h_{i,u}\right)^{-1}\quad,\quad 0\right), \tag{A5b}$$

where $j = pp$ and $j = t$ represent the permanent pycnocline and depth of the total water column, respectively. These terms arise from the vertical structure described in section 2.3.2. Note that the vertical mixing coefficient (M_V) is multiplied by d_m ($h_{i,\,pp} - h_{i,\,u}$)$^{-1}$ for ($h_{i,\,u} \le (h_{i,\,pp} - d_m)$) so that mixing occurs between the upper layer and the fluid centered at a depth of d_m below the interface.

$$H_{i,j}(q) = \frac{M_H}{w_i}\frac{h_{i-1,j}}{h_{i,j}}\left(q_{i-1,j} - q_{i,j}\right)\delta_{i,s\ell} + \frac{M_H}{w_i}\left(q_{i+1,j} - q_{i,j}\right)\,, \tag{A6}$$

where $\delta_{i,\,s\ell} = 1$ for $i = sl$ and 0 otherwise following the standard convention.

[60] The advective terms from each physical box do not generalize and are expressed in full:

$$X_{sh,u} = \frac{A}{h_{sh,u}}\left(q_{sh,l} - q_{sh,u}\right) + \frac{D}{h_{sh,u}}\left(q_{sl,u} - q_{sh,u}\right) + B_{sh} \tag{A7a}$$

$$X_{sh,l} = \frac{A}{h_{sh,l}}\left(q_{sl,l} - q_{sh,l}\right) + \frac{D}{h_{sh,l}}\left(q_{sh,u} - q_{sh,l}\right) \tag{A7b}$$

$$X_{sl,u} = \frac{A}{h_{sl,u}}\left(q_{sh,u} - q_{sl,u}\right) + \frac{D}{h_{sl,u}}\left(q_{o,u} - q_{sl,u}\right) + B_{sl} \tag{A7c}$$

$$X_{sl,l} = \frac{A}{h_{sl,l}}\left(q_{o,l} - q_{sl,l}\right) + \frac{D}{h_{sl,l}}\left(q_{sh,l} - q_{sl,l}\right)\,, \tag{A7d}$$

where B represents the buoyancy flux terms (defined in Appendix B). Definitions and values of physical parameters are presented in Table 2. The open ocean is considered an infinite source and sink with respect to the shelf and slope system.

Appendix B. Buoyancy Fluxes

[61] The shelf box buoyancy fluxes B for state variable q are

$$B_{sh} = \frac{P}{h_{sh,u}}\left(q_p - q_{sh,u}\right) + \frac{R}{h_{sh,u}}\left(q_r - q_{sh,u}\right) + \frac{C}{h_{sh,u}}\left(q_c - q_{sh,u}\right) \tag{B1a}$$

and in the surface slope box

$$B_{sl} = \frac{P}{h_{sl,u}}\left(q_p - q_{sl,u}\right)\,, \tag{B1b}$$

where P, R, and $C$are flux per length of coastline for rainfall, terrigenous runoff, and the Vancouver Island Coastal Current (VICC), respectively, with corresponding subscripts in lower case.

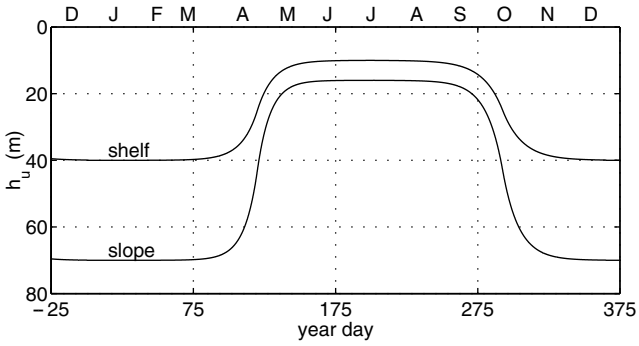

Figure C1. Seasonal variation in mixed layer depth (h_u) for shelf and slope.

Subscripts *u*, *sh*, and *sl* are upper, shelf, and slope, respectively. The coefficients vary in time for precipitation

$$P = 0.029 \exp\left\{-0.5\left[3.5 - 2\ \cos\left(\frac{2\pi}{\tau}\,(t + 20\ \text{days})\right)\right]\right\}\ \text{m d}^{-1}, \tag{B2}$$

terrigenous runoff

$$R = 0.05\ \exp\left\{-0.5\left[3.5 - 2\cos\left(\frac{2\pi}{\tau}\,(t + 20\ \text{days})\right)\right]\right\}\ \text{m d}^{-1}, \tag{B3}$$

and the VICC

$$C = 0.05 \exp\left\{-0.6\left[5 - 2\ \cos\left(\frac{2\pi}{\tau}(t + 150\ \text{days})\right)\right]\right\}\ \text{m d}^{-1}, \tag{B4}$$

where τ is 365 days and phases are relative to 1 January. We chose exponential functions to make short, steep peaks relative to a broader baseline (corresponding to data). The annual cycle of runoff volume was scaled from *Thomson et al.* [1989] to account for mixing in the inner shelf [*Ianson*, 2001]. The runoff has a low concentration of DIC (based on regressions from data in the study area [*Ianson*, 2001]), and since the area is relatively pristine, very low concentrations of organic matter are assumed. Mixing flux from the VICC (*C*) is based on peak values [*Pawlowicz and Farmer*, 1998] and a seasonal cycle from *Thomson et al.* [1989].

Appendix C. Mixed Layer Depth

[62] Annual variability in mixed layer depth was prescribed (Figure C1). Variations were added in response to prescribed storm forcing (periods of 5 and 10 days) with modulated amplitudes so that forcing was weaker during summer months:

$$\text{storm} = \left\{4\cos\left(\frac{2\pi}{10\text{d}}t\right) + \cos\left[\frac{2\pi}{5\text{d}}(t - 3\ \text{days})\right]\right\} \cdot\left\{1.2 + 0.3\cos\left[\frac{2\pi}{\tau}(t - 50\ \text{days})\right]\right\}\text{m}. \tag{C1}$$

Appendix D. Parameter Choice

[63] Biological parameters are challenging to choose. Single numbers are used to represent many processes and may also be species dependent. Often, the processes are poorly understood and nonlinear. Field measurements are difficult to make and usually scarce. We used data from many sources combined with steady state solutions of the biological model to constrain parameters. Maximum growth rates (v_m) are temperature dependent following the standard Q_{10} rule,

$$v_m = v_{m0}\ \exp\left(0.069\ \text{K}^{-1}\text{T}\right), \tag{D1}$$

where v_{m0} would be the maximum growth rate at 0 K and T is the average temperature in the upper layer. Field data [*Harrison and Platt*, 1986] were used to set growth rates. In this data compilation the saturation light intensity I_{sat} varied less than α throughout the year for similar sea surface temperatures and light intensities as in our study area, so it was kept constant in the model and α (uptake per I_{PAR} at low light intensity) was calculated from

$$\alpha = \frac{v_m(T)}{I_{\text{sat}}}\,. \tag{D2}$$

To make v_m and α independent of chl, we assumed that active phytoplankton had a C:chl ratio of 35.

[64] The particle remineralization rate (r_p) for lower layer PO matter was set using measured remineralization depth scales from sediment traps [*Martin et al.*, 1987; *Timothy and Pond*, 1997]. The depth scales were combined with the sinking rate associated with the particle flux that sediment traps measure (100 m d^{-1} [*Fowler and Knauer*, 1986]).

[65] To deal with the most poorly known parameters (e.g., the decay of the living PO pool (*s*) which represents many processes), quasi-steady state solutions were found for a simplified two-box version of the biological model (Figure 1c and (2)) [*Ianson*, 2001]. Known values (or ranges of values) of parameters and state variables were used to constrain the equations and to provide a solution for *s* and to narrow the range for the remineralization rate of DO matter (r_d).

[66] **Acknowledgments.** We thank K. Denman, K. Orians, C. S. Wong, and P. J. Harrison for many helpful discussions during the development of this model. We are also grateful to K. Denman, S. Calvert, N. Jeffery, and an anonymous reviewer for their constructive comments concerning preparation of this manuscript. This research was funded by an NSERC PGSB scholarship and by GLOBEC-Canada (supported by NSERC and Fisheries and Oceans, Canada) and by the NSERC Research grant program.

References

Alldredge, A. L., and M. W. Silver, Characteristics, dynamics and significance of marine snow, *Prog. Oceanogr.*, *20*, 41–82, 1988.

Allen, J. S., and P. A. Newberger, Downwelling circulation on the Oregon continental shelf, part I, Response to idealized forcing, *J. Phys. Oceanogr.*, *26*, 2011–2035, 1996.

Allen, J. S., P. A. Newberger, and J. Federiuk, Upwelling circulation on the Oregon continental shelf, part I, Response to idealized forcing, *J. Phys. Oceanogr.*, *25*, 1843–1866, 1995.

Bacastow, R., and E. Maier-Reimer, Dissolved organic carbon in modelling oceanic new production, *Global Biogeochem. Cycles*, *5*, 71–85, 1991.

Bienfang, P. K., P. J. Harrison, and L. M. Quarmby, Sinking rate response to depletion of nitrate, phosphate and silicate in four marine diatoms, *Mar. Biol.*, *67*, 295–302, 1982.

Bienfang, P. K., J. Szyper, and E. Laws, Sinking rate and pigment responses to light-limitation of a marine diatom: Implications to dynamics of chlorophyll maximum layers, *Oceanol. Acta*, *6*, 55–62, 1983.

Bishop, J. K., S. E. Calvert, and M. Y. S. Soon, Spatial and temporal variability of POC in the northeast subarctic Pacific, *Deep Sea Res., Part II*, *46*, 2699–2733, 1999.

Broecker, W. S., and T. H. Peng, *Tracers in the Sea*, Lamont-Doherty Earth Obs., Palisades, N. Y., 1982.

Carlson, C. A., and H. W. Ducklow, Dissolved organic carbon in the upper ocean of the central equatorial Pacific Ocean, 1992: Daily and finescale vertical variations, *Deep Sea Res., Part II*, *42*, 639–656, 1995.

Carlson, C. A., H. W. Ducklow, and A. F. Michaels, Annual flux of dissolved organic carbon from the euphotic zone in the northwestern Sargasso Sea, *Nature*, *371*, 405–408, 1994.

Christensen, J. P., Carbon export from continental shelves, denitrification and atmospheric carbon export, *Cont. Shelf Res.*, *14*, 547–576, 1994.

Crowley, T. J., Causes of climate change over the last 1000 years, *Science*, *289*, 270–277, 2000.

Denman, K. L., and M. A. Peña, A coupled 1D biological/physical model of the northeast subarctic Pacific Ocean with iron limitation, *Deep Sea Res., Part II*, *46*, 2877–2908, 1999.

Doney, S. C., Marine biogeochemical modelling challenges, *Global Biogeochem. Cycles*, *13*, 705–714, 1999.

Dugdale, R. C., and J. J. Goering, Uptake of new and regenerated forms of nitrogen in primary productivity, *Limnol. Oceanogr.*, *12*, 196–206, 1967.

Dugdale, R. C., F. P. Wilkerson, and H. J. Minas, The role of a silicate pump in driving new production, *Deep Sea Res., Part I*, *42*, 697–719, 1995.

Edwards, C. A., H. P. Batchelder, and T. M. Powell, Modeling microzooplankton and macrozooplankton dynamics within a coastal upwelling system, *J. Plankton Res.*, *22*, 1619–1648, 2000.

Eppley, R. W., and B. J. Peterson, Particulate organic matter flux and planktonic new production in the deep ocean, *Nature*, *282*, 677–680, 1979.

Fasham, M. J. R., Modelling in the marine biota, in *The Global Carbon Cycle, NATO ASI Ser., Ser. I*, *vol. 15*, edited by M. Heimann, pp. 457–504, Springer-Verlag, New York, 1993.

Fasham, M. J. R., Variations in the seasonal cycle of biological production in subarctic oceans: A model sensitivity analysis, *Deep Sea Res., Part I*, *42*, 1111–1149, 1995.

Faucher, M., W. R. Burrows, and L. Pandolfo, Empirical-statistical reconstruction of surface marine winds along the western coast of Canada, *Clim. Res.*, *11*, 173–190, 1999.

Federiuk, J., and J. S. Allen, Upwelling circulation on the Oregon continental shelf, part II, Simulations and comparisons with observations, *J. Phys. Oceanogr.*, *25*, 1867–1889, 1995.

Fowler, S. W., and G. A. Knauer, Role of large particles in the transport of elements and organic compounds through the entire water column, *Prog. Oceanogr.*, *16*, 147–194, 1986.

Freeland, H. J., and K. L. Denman, A topographically controlled upwelling center off southern Vancouver Island, *J. Mar. Res.*, *40*, 1069–1093, 1982.

Freeland, H. J., and P. McIntosh, The vorticity balance on the southern British Columbia continental shelf, *Atmos. Ocean*, *27*, 643–657, 1989.

Freeland, H. J., W. R. Crawford, and R. E. Thomson, Currents along the Pacific coast of Canada., *Atmos. Ocean*, *22*, 151–172, 1984.

Friederich, G. E., C. M. Sakamoto, J. T. Pennington, and F. P. Chavez, On the direction of the air-sea flux of CO2 in coastal upwelling systems, paper presented at Global Fluxes of Carbon and Its Related Substances in the Coastal Sea-Ocean-Atmosphere System: 1994 Sapporo IGBP Symposium, Hokkaido Univ., Sapporo Hokkaido, Japan, 1994.

Garrison, D. L., Planktonic diatoms, in *Marine Plankton Life Cycle Strategies*, edited by K. A. Steidinger and L. M. Walker, pp. 1–17, CRC Press, Boca Raton, Fla., 1984.

Haidvogel, D. B., B. J. Wilkin, and R. E. Young, A semi-spectral primitive equation ocean circulation model using vertical sigma and orthogonal curvilinear coordinates, *J. Comput. Phys.*, *94*, 151–185, 1991.

Harrison, W. G., and T. Platt, Photosynthesis-irradiance relationships in polar and temperate phytoplankton populations, *Polar Biol.*, *5*, 153–164, 1986.

Harrison, W. G., T. Platt, and M. R. Lewis, *f*-ratio and its relationship to ambient nitrate concentration in coastal waters, *J. Plankton Res.*, *9*, 235–248, 1987.

Hill, J. K., and P. A. Wheeler, Organic carbon and nitrogen in the northern California Current System: Comparison of offshore, river plume and coastally upwelled waters, *Prog. Oceanogr.*, in press, 2002.

Hsieh, W. W., D. W. Ware, and R. E. Thomson, Wind-induced upwelling along the west coast of North America, 1899–1988, *Can. J. Fish. Aquat. Sci.*, *52*, 325–34, 1995.

Hutchings, L., G. C. Pitcher, T. A. Probyn, and G. W. Bailey, The chemical and biological consequences of coastal upwelling, in *Upwelling in the Ocean: Modern Processes and Ancient Records*, edited by C. P. Summerhayeset al., pp. 65–81, John Wiley, New York, 1994.

Hutchins, D. A., and K. W. Bruland, Iron-limited diatom growth and Si:N uptake ratios in a coastal upwelling regime, *Nature*, *393*, 561–564, 1998.

Ianson, D. C., A two-dimensional carbon and nitrogen flux model in a coastal upwelling region, Ph.D. thesis, Univ. of British Columbia, Vancouver, British Columbia, Canada, 2001.

Lentz, S. J., The surface boundary layer in coastal upwelling regions, *J. Phys. Oceanogr.*, *22*, 1517–1539, 1992.

Mackas, D. L., and D. R. Yelland, Horizontal flux of nutrients and plankton across and along the British Columbia continental margin, *Deep Sea Res., Part II*, *46*, 2941–2964, 1999.

Mackenzie, R. T., A. Lerman, and L. M. Ver, Role of the continental margin in the global carbon balance during the past three centuries, *Geology*, *26*, 423–426, 1998.

Manning, M. R., Seasonal cycles in atmospheric CO_2 concentrations, in *The Global Carbon Cycle, NATO ASI Ser., Ser. I*, vol. 15, edited by M. Heimann, pp. 65–94, Springer-Verlag, New York, 1993.

Martin, J. H., G. A. Knauer, D. M. Karl, and W. W. Broenkow, VERTEX: Carbon cycling in the northeast Pacific., *Deep Sea Res.*, *34*, 267–285, 1987.

Moisan, J. R., E. E. Hoffmann, and D. B. Haidvogel, Modeling nutrient and plankton processes in the California Coastal Transition Zone, 2, A three-dimensional physical-bio-optical model, *J. Geophys. Res.*, *101*, 22,677–22,691, 1996.

Najjar, R. G., J. L. Sarmiento, and J. R. Toggweiler, Downward transport and fate of organic matter in the ocean: Simulations with a general circulation model, *Global Biogeochem. Cycles*, *6*, 45–76, 1992.

Pawlowicz, R., A tracer method for determining transport in two-layer systems, applied to the Strait of Georgia/Haro Strait/Juan de Fuca Strait estuarine system, *Estuarine Coastal Shelf Sci.*, *52*, 491–503, 2001.

Pawlowicz, R., and D. M. Farmer, Diagnosing vertical mixing in two-layer exchange flows, *J. Geophys. Res.*, *103*, 30,695–30,711, 1998.

Press, W. H., S. A. Teukolsky, W. T. Vettering, and B. P. Flannery, *Numerical Recipes in C: The Art of Scientific Computing* (2nd ed.), Cambridge Univ. Press, New York, 1992.

Redfield, A. C., B. H. Ketchum, and F. A. Richards, The influence of organisms on the composition of sea-water, in *The Sea: Ideas and Observations on Progress in the Study of the Seas*, chap. 2, pp. 26–77, John Wiley, New York, 1963.

Sakshaug, E., K. Andersen, and D. A. Kiefer, A steady state description of growth and light absorption in the marine planktonic diatom *skeletomema costatum*, *Limnol. Oceanogr.*, *34*, 198–204, 1989.

Sambrotto, R. N., G. Savidge, C. Robinson, P. Boyd, T. Takahashi, D. M. Karl, C. Langdon, D. Chipman, J. Marra, and L. Codispoti, Elevated consumption of carbon relative to nitrogen in the surface ocean, *Nature*, *363*, 248–250, 1993.

Sarmiento, J. L., Biogeochemical ocean models, in *Climate System Modelling*, edited by K. E. Trenberth, pp. 519–551, Cambridge Univ. Press, New York, 1992.

Sarmiento, J. L., R. D. Slater, M. J. R. Fasham, H. W. Ducklow, J. R. Toggweiler, and G. T. Evans, A seasonal three-dimensional ecosystem model of nitrogen cycling in the North Atlantic euphotic zone, *Global Biogeochem. Cycles*, *7*, 417–450, 1993.

Siegenthaler, U., and J. L. Sarmiento, Atmospheric carbon dioxide and the ocean, *Nature*, *365*, 119–125, 1993.

Simpson, J. J., Processes affecting upper ocean chemical structure in an eastern boundary current, in *Dynamic Processes in the Chemistry of the Upper Ocean*, edited by J. D. Burton, P. G. Brewer, and R. Chesselet, pp. 53–77, Plenum, New York, 1986.

Simpson, J. J., and A. Zirino, Biological control of pH in the Peruvian coastal upwelling area, *Deep Sea Res.*, *27*, 733–744, 1980.

Skirrow, G., The dissolved gases—Carbon dioxide, in *Chemical Oceanography*, vol. 2, edited by J. P. Riley and G. Skirrow, pp. 1–192, Academic, San Diego, Calif., 1975.

Smetacek, V. S., Role of sinking in diatom life-history cycles: Ecological, evolutionary and geological significance, *Mar. Biol.*, *84*, 239–251, 1985.

Smith, R. L., The physical processes of coastal ocean upwelling systems, in *Upwelling in the Ocean: Modern Processes and Ancient Records*, edited by C. P. Summerhayeset al., pp. 39–64, John Wiley, 1994.

Smith, S. V., and J. T. Hollibaugh, Coastal metabolism and the oceanic organic carbon cycle, *Rev. Geophys.*, *31*, 75–89, 1993.

Sverdrup, H. U., On conditions for the vernal blooming of phytoplankton, *J. Cons. Int. Explor. Mer.*, *18*, 287–295, 1953.

Taylor, A. H., R. J. Geider, and F. J. Gilbert, Seasonal and latitudinal dependencies of phytoplankton carbon-to-chlorophyll a ratios: results of a modelling study, *Mar. Ecol. Prog. Ser.*, *152*, 51–66, 1997.

Thomson, R. E., and D. Ware, A current velocity index of ocean variability, *J. Geophys. Res.*, *101*, 14,297–14,310, 1996.

Thomson, R. E., B. M. Hickey, and P. H. LeBlond, The Vancouver Island Coastal Current: Fisheries barrier and conduit, in *Effects of Ocean Variability on Recruitment and an Evaluation of Parameters Used in Stock Assessment Models*, edited by G. A. McFarlane, *Spec. Publ. Can. Fish. Aquat. Sci., 108*, 265–296, 1989.

Timothy, D. A., and S. Pond, Describing additional fluxes to deep sediment traps and water-column decay in a coastal environment, *J. Mar. Res.*, *55*, 383–406, 1997.

Tsunogai, S., S. Watanabe, and T. Sato, Is there a "continental shelf pump" for the absorption of atmospheric CO_2?, *Tellus, Ser. B*, *51*, 701–712, 1999.

Volk, T., and M. I. Hoffert, Ocean carbon pumps: Analysis of relative strengths and efficiencies in ocean-driven atmospheric pCO_2 changes, in *The Carbon Cycle and Atmospheric CO_2, Natural Variations Archaen to Present, Geophys. Monogr. Ser.*, vol. 32, edited by E. T. Sundqvist and W. S. Broecker, pp. 99–110, AGU, Washington, D. C., 1985.

Wanninkhof, R., Relationship between gas exchange and wind speed over the ocean, *J. Geophys. Res.*, *97*, 7373–7382, 1992.

Watson, A., Air-sea gas exchange and carbon dioxide, in *The Global Carbon Cycle, NATO ASI Ser., Ser. I*, vol. 15, edited by M. Heimann, pp. 397–411, Springer-Verlag, New York, 1993.

Weiss, R., Carbon dioxide in water and seawater: The solubility of a non-ideal gas, *Mar. Chem.*, *2*, 203–215, 1974.

Whitney, F. A., and H. J. Freeland, Variability in upper-ocean water properties in the NE Pacific Ocean, *Deep Sea Res., Part II*, *46*, 2351–2370, 1999.

Whitney, F. A., C. S. Wong, and P. W. Boyd, Interannual variability in nitrate supply to surface waters of the Northeast Pacific Ocean, *Mar. Ecol. Prog. Ser.*, *170*, 15–23, 1998.

Wong, C. S., Y. Zhiming, W. K. Johnson, R. J. Matear, and F. A. Whitney, Dynamics and characterization of marine organic matter, in *Professor Handa's Retirement Commemorative Volume*, edited by N. Handa, E. Tanoue, and T. Hama, pp. 107–116, Terra Sci., Tokyo, 1997.

Wroblewski, J. S., A model of phytoplankton plume formation during variable Oregon upwelling, *J. Mar. Res.*, *35*, 357–394, 1977.

S. E. Allen, Oceanography, Earth and Ocean Sciences Department, University of British Columbia, 6270 University Boulevard, Vancouver, BC V6T 1Z4, Canada. (allen@eos.ubc.ca)

D. Ianson, Department of Oceanography, Texas A&M University, College Station, TX 77843-3146, USA. (ianson@halodule.tamu.edu)